Aeroelastic simulations of wind turbine using 13 DOF rigid beam model

Sudhakar Gantasala, Jean-Claude Luneno, Jan-Olov Aidanpää, Michel Cervantes

Aeroelastic simulations of wind turbine using 13 DOF rigid beam model

Sudhakar Gantasala*, Jean-Claude Luneno, Jan-Olov Aidanpää, Michel Cervantes

ISROMAC 2016

International Symposium on Transport Phenomena and Dynamics of Rotating Machinery

Hawaii, Honolulu

April 10-15, 2016

Abstract

The vibration behavior of wind turbine substructures is mainly dominated by their first few vibration modes because wind turbines operate at low rotational speeds. In this study, 13 degrees of freedom (DOF) model of a wind turbine is derived considering fundamental vibration modes of the tower and blades which are modelled as rigid beams with torsional springs attached at their root. Linear equations of motion (EOM) governing the structural behavior of wind turbines are derived by assuming small amplitude vibrations. This model is used to study the coupling between the structural and aerodynamic behavior of NREL 5 MW model wind turbine. Aeroelastic natural frequencies of the current model are compared with the results obtained from the finite element model of this wind turbine. Quasi-steady aerodynamic loads are calculated considering wind velocity changes due to height and tower shadow effects. In this study, vibration responses are simulated at various wind velocities. The derived 13 DOF simplified model of the wind turbine enables to simulate the influence of change in parameters and operating conditions on vibration behavior with less computational effort. Besides that, the results of the simplified models can be interpreted with much ease.

Keywords

Aeroelastic – Wind turbine – Rigid beam

Department of Engineering Sciences and Mathematics, Luleå University of Technology, Luleå, Sweden

***Corresponding author**: sudhakar.gantasala@ltu.se

INTRODUCTION

Wind turbine structures consist of both rotating and non-rotating substructures manufactured in different materials. In order to perform a dynamic analysis of wind turbines, detailed structural model along with loads predicted from the aerodynamic analysis of the blades are needed. Dynamic changes in the wind and rotational effects force flexible blades to vibrate. Rotation and vibrations of the blades change the effective wind velocity generating aerodynamic loads. Thus the structural and aerodynamic analyses of the wind turbine are coupled to each other, dynamic behavior of the wind turbine structures can be accurately predicted considering this coupling. Finite element methods (FEM) can be used to model structural behavior and computational fluid dynamics (CFD) techniques are used for predicting aerodynamic loads. Coupled structural and aerodynamic analysis using detailed FEM and CFD models is computationally expensive for parametric studies in the design stage. To determine the influence of this coupling on the vibration behavior, simple models for structural and aerodynamic calculations are used in this study.

In literature, rigid and flexible beam models are used to analyze the dynamics of the isolated rotating blades considering pitch, flap, and lead-lag vibrations. Chopra [1,2] considered rigid wind turbine blades with root hinges and analyzed its linear and nonlinear dynamic behavior with and without external loadings. Kim and Lee [3] considered a simple structural model for wind turbine with only 10 degrees of freedom (DOF). They analyzed the effect of asymmetry in the blade stiffnesses on the system stability over a range of rotational speeds. Ramakrishnan and Feeny [4] modeled wind turbine blade as a non-linear flexible beam and reduced its equation of motion to a nonlinear Mathieu equation to study super-harmonic resonances. Wind turbine blades are made of aerofoil cross sections which are twisted and tapered along the blade length. The vibration behavior in bending and torsion are therefore coupled. Kim and Lee [5] derived the equations of motion for coupled flapping, lead-lag and torsional vibrations of pre-twisted wind turbine blades. They calculated modal frequencies of the blade using the assumed modeshape method.

Fundamental vibration modes of all the substructures contribute more to the dynamic response of the wind turbine than the other higher frequency vibration modes because wind turbines operate at low rotational speeds. In this study, 13 DOF model of the wind turbine structure is derived considering fundamental vibration modes of all the substructures. Tower and blades are modeled as rigid beams with equivalent inertias and supported by springs at their roots. This configuration duplicates first bending vibration modes of the substructures through the deformation of the torsional spring (as shown in Fig. 1). Lagrange's equations are used to derive the equations of motion (EOM) for a three blade horizontal axis wind turbine. MATLAB symbolic math toolbox is used to derive the EOM. Turbine components like the hub and nacelle are assumed to be rigid bodies. Tower and blades kinetic energies are calculated considering their distributed mass properties. Small amplitude vibrations are assumed for all the DOF and EOM are linearized by retaining only the first order terms. Structural modeling of the wind turbine stationary and rotating substructures together will yield coupled nonlinear differential equations with periodic coefficients irrespective of the type of the reference coordinate frame. Periodic coefficients of the linear differential equations for symmetric blades can be eliminated by using multi-blade coordinate transformation [3,6] and eigenvalue analysis can be used to calculate natural frequencies of the structure. MBC transformation models collective blades motion in the stationary frame of reference. For symmetric blades, MBC transformation yields constant coefficients in the EOM if the gravity effect of the rotating blades is ignored. The influence of the gravity on natural frequencies can be ignored [5]. Blade element momentum (BEM) theory [7] is used for calculating quasi-steady aerodynamic loads acting on the blades. Wind shear is modeled using wind profile power law using mean wind velocity at nacelle height. Tower shadow is modeled using potential theory of flow around a cylinder for calculating wind velocity near the tower [7]. NREL 5 MW model wind turbine data [8,9] is considered as an example for this study. Aeroelastic natural frequencies of this 13 DOF rigid beam model in the operating wind velocity range of 3-25 m/s are compared with the results predicted from the FEM model of this wind turbine [10]. Vibration responses of the 13 DOF model are simulated at various wind velocities using the operating parameters like rotating speeds, pitch angles of the NREL 5 MW model wind turbine [8] and considering aerodynamic coupling with structural behavior. In this study, variations in the wind velocity due to wind shear and tower shadow are only considered. Thus the spectral vibration responses of the 13 DOF model consist of frequencies 1P, 3P (P refers to the rotational frequency) and their harmonics.

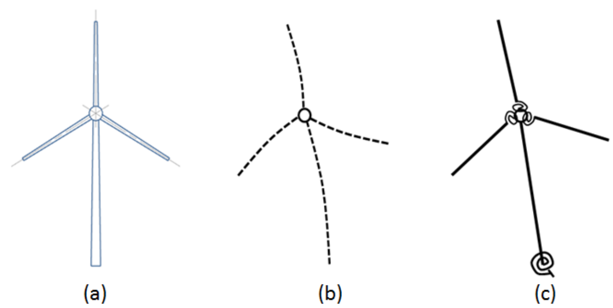

Figure 1. Wind turbine: (a) geometric model, (b) flexible beam model, (c) rigid beam model

1. STRUCTURAL MODEL

Geometric model of the wind turbine with the considered degrees of freedom of the substructures is shown in Fig. 2(a). Reference coordinate system OXYZ is fixed at the base of the tower which is used to derive the EOM. The tower can oscillate about X and Y axes at the origin O with DOF's α and β respectively, which are known as tower fore-aft and side-to-side vibrations. Hub and nacelle are considered as two rigid masses with their center of gravity (C.G.) locations C and B at distances l_h and l_n respectively from the yaw axis (point A). These two bodies are fixed on top of the tower and can rotate relative to the tower about the yaw axis with a DOF γ. The nacelle is a stationary part which encloses the generator and other systems. The generator has both stationary and rotating parts. The generator rotor is connected to the hub through a gearbox. In this model, inertias of the generator rotor and the hub are lumped to a single inertia and attached to an equivalent drive shaft. Torsional vibration of the equivalent drive shaft is denoted as ψ . Blade vibrates with in-plane (lead-lag), out-of-plane (flap) and torsional DOF $\theta_i, \varphi_i, \varepsilon_i$ (i refers to the blade number) respectively. These motions are defined about a local coordinate system $x_{bi}y_{bi}z_{bi}$ fixed at the root of the blade as shown in Fig. 2(a). Position vectors are defined initially and then energy equations for all the substructures are obtained to derive the EOM using Lagrange's equations. Kinetic energy is denoted by KE and potential energy is denoted by PE.

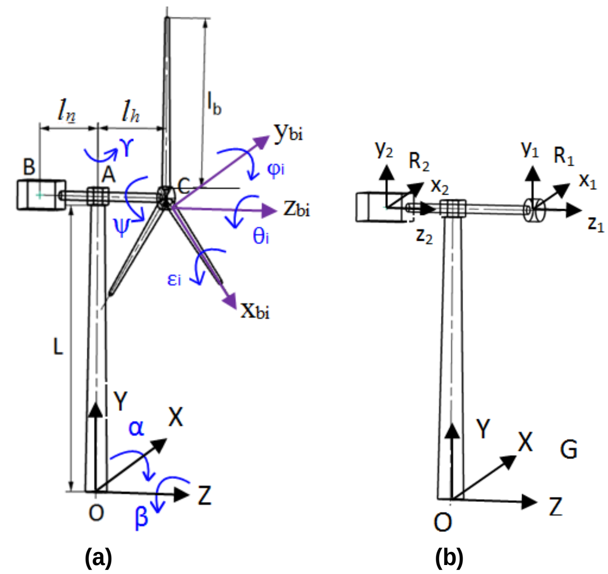

Figure 2. (a) Geometric model of the wind turbine structure with the considered DOF in the model, (b) Hub and nacelle local coordinate systems in which inertia of masses are defined

1.1 Tower:

As the tower cross section changes along the length, kinetic energy of a small element of length dy located at a distance y from the origin O along the axis Y is defined initially and it is integrated over the full length of the tower to calculate total kinetic energy of the tower. Position vector of a small element of length dy is defined below.

$$\vec{q}_{tower} = T_X(\alpha)\, T_Z(\beta) \begin{Bmatrix} 0 \\ y \\ 0 \end{Bmatrix} \tag{1}$$

where $T_X(\alpha)$ and $T_Z(\beta)$ are the transformation matrices about X and Z axis (given in Appendix).

Kinetic, potential energies of the tower and generalized dissipative forces due to damping are given below.

$$\begin{aligned} KE_{tower} &= \int_0^L \frac{1}{2} (\rho A_{tower}) \left| \frac{d\vec{q}_{tower}}{dt} \right|^2 dy \\ PE_{tower} &= \frac{1}{2} K_\alpha \alpha^2 + \frac{1}{2} K_\beta \beta^2 + \int_0^L (\rho A_{tower})\, g\, \vec{q}_{tower\,(Y)}\, dy \\ Q_\alpha &= C_\alpha \dot{\alpha}, \quad Q_\beta = C_\beta \dot{\beta} \end{aligned} \tag{2}$$

where KE_{tower} and PE_{tower} are the kinetic and potential energies of the tower; L is the length of the tower; Q_α and Q_β are the generalized forces; ρA_{tower} is mass per unit length of the tower; $\vec{q}_{tower_{(Y)}}$ is the Y coordinate of the position vector of the tower; g is acceleration due to gravity; K_α, K_β and C_α, C_β are stiffness, damping coefficients of the springs and dampers restricting tower vibrations α, β.

1.2 Hub and Nacelle:

A hub is a joint that connects turbine blades to the rotating shaft and transfers energy to the generator through the gearbox. In this model, hub rotating on the low speed shaft and generator rotating on the high speed shaft are modeled as a single inertia. This equivalent inertia mass rotates with an angular velocity of ω and undergoes torsional oscillations on an equivalent drive shaft whose torsional stiffness and damping coefficients are known. As this equivalent inertia mass is located on top of the tower, gyroscopic moments are generated in the system due to the change in orientation of its angular velocity vector due to the tower vibrations and yaw motion. Rotational kinetic energy of the equivalent inertia mass accounts for the gyroscopic moments which are calculated using inertia tensor defined about its C.G. and angular velocity vector defined in the local coordinate system $R_1:x_1y_1z_1$ as shown in Fig. 2(b). The order of rotations followed to get the position vector is $\alpha,\beta,\gamma,(\omega t+\psi)$ respectively and the same rotation order is used to transform the velocity vectors $\dot{\alpha},\dot{\beta},\dot{\gamma}$ into the $R_1:x_1y_1z_1$ coordinate system. Position, angular velocity vectors, energy expressions of the rigid hub and nacelle masses and generalized dissipative forces due to damping are given in Eq. (3) & (4).

$$\vec{q}_h = T_X(\alpha)\ T_Z(\beta)\ T_Y(\gamma)\begin{Bmatrix}0\\ L_1\\ l_h\end{Bmatrix}$$

$$\vec{\Omega}_h = \begin{Bmatrix}0\\ 0\\ \omega+\dot{\psi}\end{Bmatrix} + T_Z^T(\omega t+\psi)\begin{Bmatrix}0\\ \dot{\gamma}\\ 0\end{Bmatrix} + T_Z^T(\omega t+\psi)\ T_Y^T(\gamma)\begin{Bmatrix}0\\ 0\\ \dot{\beta}\end{Bmatrix}$$

$$+T_Z^T(\omega t+\psi)\ T_Y^T(\gamma)\ T_Z^T(\beta)\begin{Bmatrix}\dot{\alpha}\\ 0\\ 0\end{Bmatrix} \qquad (3)$$

$$KE_{hub} = \frac{1}{2}m_h\left|\frac{d\vec{q}_h}{dt}\right|^2 + \frac{1}{2}\vec{\Omega}_h^{\ T}\begin{bmatrix}ID_h & 0 & 0\\ 0 & ID_h & 0\\ 0 & 0 & IP_1\end{bmatrix}\vec{\Omega}_h$$

$$PE_{hub} = \frac{1}{2}K_\gamma\gamma^2 + \frac{1}{2}K_\psi\psi^2 + m_h\ g\ \vec{q}_{h(Y)}$$

$$Q_\gamma = C_\gamma\dot{\gamma}, \qquad Q_\psi = C_\psi\dot{\psi}$$

$$\vec{q}_n = T_X(\alpha)\ T_Z(\beta)\ T_Y(\gamma)\begin{Bmatrix}0\\ L_1\\ -l_n\end{Bmatrix}$$

$$\vec{\Omega}_n = \begin{Bmatrix}0\\ \dot{\gamma}\\ 0\end{Bmatrix} + T_Y^T(\gamma)\begin{Bmatrix}0\\ 0\\ \dot{\beta}\end{Bmatrix} + T_Y^T(\gamma)\ T_Z^T(\beta)\begin{Bmatrix}\dot{\alpha}\\ 0\\ 0\end{Bmatrix} \qquad (4)$$

$$KE_{nacelle} = \frac{1}{2}m_n\left|\frac{d\vec{q}_n}{dt}\right|^2 + \frac{1}{2}\vec{\Omega}_n^{\ T}\begin{bmatrix}ID_n & 0 & 0\\ 0 & ID_n & 0\\ 0 & 0 & IP_n\end{bmatrix}\vec{\Omega}_n$$

$$PE_{nacelle} = m_n\ g\ \vec{q}_{n(Y)}$$

where $\vec{q}_h$, $\vec{q}_n$ and $\vec{\Omega}_h, \vec{\Omega}_n$ are the position, angular velocity vectors of the hub and nacelle masses m_h, m_n respectively; $T_Y(\gamma)$ and $T_Z(\omega t+\psi)$ are the transformation matrices about Y and Z axis (given in Appendix); KE_{hub}, $KE_{nacelle}$, PE_{hub}, $PE_{nacelle}$ are the kinetic and potential energies of the hub and nacelle masses; ID_h, ID_n are transverse mass moment of inertias of the hub and nacelle masses about the local coordinate system defined at their mass centers (shown in Fig. 2(b)) parallel to OXYZ coordinate system; IP_1 is the sum of hub and generator polar moment of inertias about the low speed shaft $IP_h, IP_{Gen_{LSS}}$; IP_n is the nacelle polar moment of inertia; L_1 is the distance of hub rotational axis above the ground along the tower centerline; $\vec{q}_{h(Y)}, \vec{q}_{n(Y)}$ are the Y coordinates of the position vectors of the hub and nacelle C.G.; K_γ and C_γ are stiffness and damping coefficients of the springs and dampers of the yaw actuation system which control relative position of the rigid hub and nacelle mass assembly with respect to tower; K_ψ and C_ψ are stiffness and damping coefficients of the equivalent drive shaft.

1.3 Blades:

Blade in-plane (lead-lag) vibrations defined about z_{bi} axis of the rotating coordinate system placed at the root of the blade are denoted by θ_i, out-of-plane (flap) vibrations defined about y_{bi} axis are denoted by φ_i and torsional vibrations defined about x_{bi} axis are denoted by ε_i (refer Fig. 2(a)), where $i = 1,2,3$ denote the blade number. The kinetic energy of the blade is obtained by integrating the kinetic energy of a small element of length dr located at a radial distance of r from the blade root, over the full length of the blade (l_b). Position vector of the small element dr is given below.

$$\vec{q}_{b_i} = T_X(\alpha)\,T_Z(\beta)\,T_Y(\gamma)\left(\begin{Bmatrix}0\\ L_1\\ l_h\end{Bmatrix} + T_Z(\omega t+\psi)\begin{Bmatrix}r_h\\ 0\\ 0\end{Bmatrix} + T_Z(\omega t+\psi)T_Z(\theta_i)T_Y(\varphi_i)T_X(\varepsilon_i)\begin{Bmatrix}r\\ cg_y\\ cg_z\end{Bmatrix}\right) \qquad (5)$$

where $T_Z(\theta_i), T_Y(\varphi_i), T_X(\varepsilon_i)$ are the transformation matrices given in the Appendix; (r, cg_y, cg_z) are the coordinates of the C.G. of the blade section in local coordinate system $x_{bi}y_{bi}z_{bi}$.

Energy expressions for the i^{th} blade are given below.

$$KE_{b_i} = \int_0^{l_b} \frac{1}{2}(\rho A_{blade}) \left|\frac{d\vec{q}_{b_i}}{dt}\right|^2 dr$$

$$PE_{b_i} = \frac{1}{2} K_{\theta_i} \theta_i^2 + \frac{1}{2} K_{\varphi_i} \varphi_i^2 + \frac{1}{2} K_{\varepsilon_i} \varepsilon_i^2 + \int_0^{l_b} (\rho A_{blade})\, g\, \vec{q}_{b_{i(Y)}}\, dr \tag{6}$$

$$Q_{b_{\theta i}} = C_{\theta_i} \dot{\theta}_i$$

$$Q_{b_{\varphi i}} = C_{\varphi_i} \dot{\varphi}_i$$

$$Q_{b_{\varepsilon i}} = C_{\varepsilon_i} \dot{\varepsilon}_i$$

where $KE_{b_i}, PE_{b_i}, Q_{b_{\theta i}}, Q_{b_{\varphi i}}, Q_{b_{\varepsilon i}}$ are the kinetic, potential energies and generalized forces of the i^{th} blade; ρA_{blade} is the mass per unit length of the blade; $\vec{q}_{b_{i(Y)}}$ is the Y coordinate of the position vector of the i^{th} blade; $K_{\theta_i}, K_{\varphi_i}, K_{\varepsilon_i}$ and $C_{\theta_i}, C_{\varphi_i}, C_{\varepsilon_i}$ are stiffness, damping coefficients of the springs and dampers restricting i^{th} blade in-plane, out-of-plane, torsional vibrations $\theta_i, \varphi_i, \varepsilon_i$.

Total kinetic and potential energies of the system are obtained by summing up individual contributions from all the substructures.

$$KE = KE_{tower} + KE_{hub} + KE_{nacelle} + \sum_{i=1}^{3} KE_{b_i}$$

$$PE = PE_{tower} + PE_{hub} + PE_{nacelle} + \sum_{i=1}^{3} PE_{b_i} \tag{7}$$

Equations of motion are derived from the total energy expressions of the system using Lagrange's equations given in Eq. (8) for all the generalized coordinates.

$$\frac{d}{dt}\left(\frac{\partial(KE)}{\partial \dot{q}_j}\right) - \frac{\partial(KE)}{\partial q_j} + \frac{\partial(PE)}{\partial \dot{q}_j} + Q_{q_j} = 0 \tag{8}$$

where q_j → generalized coordinates $\alpha, \beta, \gamma, \psi, \theta_i, \varphi_i, \varepsilon_i$

$(i = 1,2,3)$

Equations of motion obtained from the Eq. (8) are coupled nonlinear differential equations in the generalized coordinates. In the current work, small amplitude vibrations are assumed and linear EOM are obtained after retaining first order terms. Linear EOM in the matrix form is given in Eq. (9) and whose matrices contain periodic terms.

$$M(\omega t)\{\ddot{q}(t)\} + C(\omega t)\{\dot{q}(t)\} + K(\omega t)\{q(t)\} = \{f(t)\} \tag{9}$$

where $M(\omega t)$, $C(\omega t)$, $K(\omega t)$ are the system matrices,

$\{q(t)\} = [\alpha, \beta, \gamma, \psi, \theta_1, \theta_2, \theta_3, \varphi_1, \varphi_2, \varphi_3, \varepsilon_1, \varepsilon_2, \varepsilon_3]^T$ and

$\{f(t)\}$ is the force vector

Rotating blade's DOF are transformed into multi blade coordinates [6] using the transformation matrix given in Eq. (10).

$$T = \begin{bmatrix} I_4 & 0 & 0 & 0 \\ 0 & T_B(\omega t) & 0 & 0 \\ 0 & 0 & T_B(\omega t) & 0 \\ 0 & 0 & 0 & T_B(\omega t) \end{bmatrix} \tag{10}$$

where,

$$T_B(\omega t) = \begin{bmatrix} 1 & cos(\xi_1) & sin(\xi_1) \\ 1 & cos(\xi_2) & sin(\xi_2) \\ 1 & cos(\xi_3) & sin(\xi_3) \end{bmatrix},$$

$$\xi_1 = \omega t,\ \xi_2 = \omega t + \frac{2\pi}{3},\ \xi_3 = \omega t + \frac{4\pi}{3}$$

and I_4 is a 4x4 identity matrix which retains first four non-rotating DOF as it is in the final transformed coordinate vector. ξ_1, ξ_2, ξ_3 are the instantaneous azimuthal positions of the blades with respect to a fixed reference. The blades are placed symmetrically around the circumference of the hub.

The relationship between $\{q(t)\}$ and multi-blade coordinate's vector $\{q_B(t)\}$ is given in Eq. (11).

$$\{q(t)\} = T\,\{q_B(t)\} \tag{11}$$

where

$\{q_B(t)\} = [\alpha, \beta, \gamma, \psi, \theta_0, \theta_c, \theta_s, \varphi_0, \varphi_c, \varphi_s, \varepsilon_0, \varepsilon_c, \varepsilon_s]^T$

Difference between $\{q(t)\}$ and $\{q_B(t)\}$ is only in the blades in-plane, out-of-plane and torsional vibrations. Subscripts *0, c, s* refer to collective, progressive and regressive modes of the blade assembly which can excite tower vibration modes. In collective mode, the vibrations of the blades are in phase with each other, whereas in the progressive and regressive modes, phase difference exists between blade vibrations as defined in the matrix $T_B(\omega t)$. Detailed explanation of these coordinates and MBC transformations are given in [6]. The EOM obtained after MBC transformation in the matrix form are given in Eq. (12).

$$M_B(\omega t)\{\ddot{q}_B(t)\} + C_B(\omega t)\{\dot{q}_B(t)\} + K_B(\omega t)\{q_B(t)\} = \{f_B(t)\} \tag{12}$$

where

$$M_B(\omega t) = T^T M(\omega t) T, \quad C_B(\omega t) = T^T C(\omega t) T + 2\, T^T M(\omega t) \dot{T},$$
$$K_B(\omega t) = T^T K(\omega t) T + T^T C(\omega t) \dot{T} + T^T M(\omega t) \ddot{T}, \quad f_B(t) = T^T f(t)$$

Gravity effect changes stiffness over the azimuthal rotation of the blade [5] which makes K_B matrix still periodic in time even after MBC transformation. Neglecting gravity term makes the system matrices time invariant for symmetric blades, and therefore eigenvalue analysis can be used to calculate natural frequencies. However, for asymmetric blades, time invariant system matrices cannot be obtained using MBC transformation even after neglecting gravity terms.

Data required to simulate the derived 13 DOF model are computed from the structural details of NREL 5 MW model wind turbine. The inertia properties of all the subsystems can be calculated from the data given in [8,9]. Fundamental vibration modes of all the subsystems obtained from the FEM analysis of this wind turbine structure are also reported in these references. Using the natural frequencies and inertia properties reported in [8,9], unknown equivalent spring stiffness coefficients for vibration DOF α, β, $\theta_i, \varphi_i, \varepsilon_i$ are calculated.

2. AERODYNAMIC MODEL

Beam element momentum (BEM) theory [7] is used to calculate aerodynamic loads considering wind shear and tower shadow effects. Wind shear is modeled using wind profile power law using mean wind velocity at nacelle height and a parameter of 0.2 for the amount of shear. Tower shadow is modeled using potential theory of flow around a cylinder [7]. The tower diameter variation along its height is also taken into account in the calculation of the wind velocity near the tower. Prandtl's tip loss factor and Glauert corrections are considered in the BEM theory used in this study. Aerodynamic loads are calculated at the aerodynamic center of the aerofoil sections of the blade. Velocity triangle without and with considering blade vibrations are shown in Fig. 3.

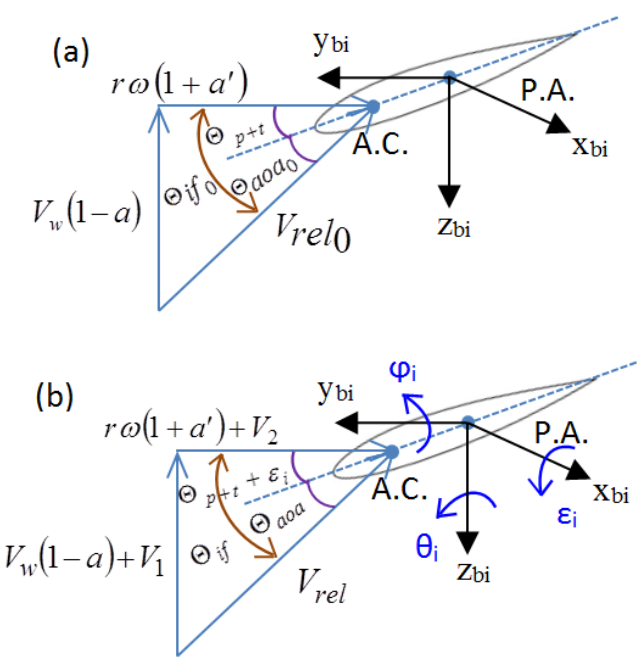

Figure 3. Velocity triangle at the blade section (a) without and (b) with considering blade vibrations

Expressions for the inflow angle, angle of attack without considering blade vibrations are given in Eq. (13) & (14).

$$\Theta_{if_0} = tan^{-1}\left(\frac{V_w(1-a)}{r\omega(1+a')}\right) \quad (13)$$

$$\Theta_{aoa_0} = \Theta_{if_0} - \Theta_{p+t} \quad (14)$$

where, $\Theta_{if_0}, \Theta_{aoa_0}$ are the inflow angle and angle of attack, ignoring the blade vibrations; Θ_{p+t} is the sum of blade pitch and section twist angles; V_w and ω are the wind velocity and rotational frequency of the blade; r is the radial distance of the blade section from the hub center; a and a' are the axial and tangential induction factors.

Blade vibration velocities change the relative velocity of wind entering the blade section as shown in Fig. 3(b). As the structural model of the blade is built with respect to pitch axis, due to the offset between aerodynamic center and pitch axis, both the inflow angle and the angle of attack (AOA) depend on torsional vibrations. Expressions for the inflow angle, angle of attack considering blade vibrations are given in Eq. (15) & (16).

$$\Theta_{if} = tan^{-1}\left(\frac{V_w(1-a)+V_1}{r\omega(1+a')+V_2}\right) \quad (15)$$

where,

$$V_1 = -r\dot{\varphi}_i + a_{AC}\cos(\Theta_{p+t}+\varepsilon_i)\dot{\varepsilon}_i$$
$$V_2 = r\dot{\theta}_i - a_{AC}\sin(\Theta_{p+t}+\varepsilon_i)\dot{\varepsilon}_i$$

$$\Theta_{aoa} = \Theta_{if} - (\Theta_{p+t}+\varepsilon_i) \quad (16)$$

where, $\Theta_{if}, \Theta_{aoa}$ are the inflow angle and angle of attack considering blade vibrations; $\dot{\theta}_i, \dot{\varphi}_i, \dot{\varepsilon}_i$ are the velocities of the i^{th} blade in-plane, out-of-plane and torsional vibrations; ε_i is the i^{th} blade torsional vibration; a_{AC} is the distance between the aerodynamic center (A.C.) and pitch axis (P.A.) (shown in Fig. 3) of the blade section.

Change in the AOA due to blade vibrations can be approximated according to Eq. (17).

$$\begin{aligned}\Delta\Theta &= \Theta_{aoa} - \Theta_{aoa0} \\ &\approx \frac{r\omega(1+a')}{V_{rel_0}^2}V_1 - \frac{V_w(1-a)}{V_{rel_0}^2}V_2 - \varepsilon_i\end{aligned} \quad (17)$$

Lift, drag and pitching moment coefficients at Θ_{aoa} can be expanded using Taylor series expansion about the Θ_{aoa_0} as given in Eq. (18).

$$\begin{aligned}C_L(\Theta_{aoa}) &\approx C_L(\Theta_{aoa_0}) + C_L'(\Theta_{aoa_0})\Delta\Theta \\ C_D(\Theta_{aoa}) &\approx C_D(\Theta_{aoa_0}) + C_D'(\Theta_{aoa_0})\Delta\Theta \\ C_M(\Theta_{aoa}) &\approx C_M(\Theta_{aoa_0}) + C_M'(\Theta_{aoa_0})\Delta\Theta\end{aligned} \quad (18)$$

where, C_L, C_D, C_M are the lift, drag and moment coefficients of the aerofoil; C_L', C_D', C_M' are the slopes of the lift, drag and moment coefficient curves.

Aerodynamic loads considering these coefficients are expressed in Eq. (19)-(21) where, if written in matrix form the coefficients of the variables $\dot{\theta}_i, \dot{\varphi}_i, \dot{\varepsilon}_i, \varepsilon_i$ can be separated into matrices C_{Aero} and K_{Aero} which are known as aerodynamic damping and stiffness matrices.

$$\begin{aligned}L \approx\ & \frac{1}{2}\rho c V_{rel_0}^2 C_L(\Theta_{aoa_0}) \\ & + \frac{1}{2}\rho c C_L'(\Theta_{aoa_0})\left\{r\omega(1+a')V_1 - V_w(1-a)V_2 - V_{rel_0}^2\varepsilon_i\right\}\end{aligned} \quad (19)$$

$$
\begin{aligned}
D \approx{}& \frac{1}{2}\rho c V_{rel_0}^2 C_D\left(\Theta_{aoa_0}\right) \\
&+ \frac{1}{2}\rho c C_D'\left(\Theta_{aoa_0}\right)\left\{r\omega(1+a')V_1 - V_w(1-a)V_2 - V_{rel_0}^2 \varepsilon_i\right\}
\end{aligned}
\tag{20}
$$

$$
\begin{aligned}
M \approx{}& \frac{1}{2}\rho c^2 V_{rel_0}^2 C_M\left(\Theta_{aoa_0}\right) \\
&+ \frac{1}{2}\rho c^2 C_M'\left(\Theta_{aoa_0}\right)\left\{r\omega(1+a')V_1 - V_w(1-a)V_2 - V_{rel_0}^2 \varepsilon_i\right\}
\end{aligned}
\tag{21}
$$

The aerodynamic loads in Eq. (19)-(21) are introduced in the structural model given in Eq. (9) and the EOM considering structural and aerodynamic coupling is given in Eq. (22). Aeroelastic natural frequencies can be calculated by transforming $\{q(t)\}$ in Eq. (22) to multi-blade coordinates $\{q_B(t)\}$ and using the eigenvalue analysis of the system.

$$
\begin{aligned}
M(\omega t)\,\{\ddot{q}(t)\} &+ \left[C(\omega t)+C_{Aero}\right]\{\dot{q}(t)\} \\
&+ \left[K(\omega t)+K_{Aero}\right]\{q(t)\} = \{f(t)\}+\{f_{Aero}(t)\}
\end{aligned}
\tag{22}
$$

3. RESULTS AND DISCUSSION

Data of the model wind turbine [8] are inserted into the system of Eq. (12) and eigenvalues are obtained at zero speed and by ignoring gravity terms. Natural frequencies of the present 13 DOF model are compared with the values predicted using FAST (aeroelastic simulation tool) [8] in Table 1. As FAST doesn't model blade torsional vibrations its natural frequency in the current rigid beam model is compared with the frequency value predicted in [5] where blade is modeled using FEM. Natural frequencies calculated using these two models (FEM vs. 13 DOF model) at zero speed match well and thus this 13 DOF model can be considered as a good representation of dynamic behavior of the wind turbine structure in the low frequency vibration modes.

NREL 5 MW wind turbine operates over a wind velocity range of 3-25 m/s and its rotational speed increases from 7.35 rpm at a wind velocity of 3 m/s to 12.1 rpm at a wind velocity of 11.4 m/s and operates at this rotational speed till 25 m/s wind velocity by changing pitch angle of the blades [8]. Natural frequencies of the 13 DOF model considering only the rotational speed variation with wind velocities between 3-25 m/s are shown in Fig. 4. Natural frequencies of the blade DOF change till 11.4 m/s wind velocity due to increase in rotational speed and thereafter remains constant as there is no change in the rotational speed. Aerodynamic loads calculated for mean wind velocities in the range between 3-25 m/s at the nacelle are used to determine aeroelastic natural frequencies of this model which are plotted in Fig. 5. Differences in the natural frequencies in Fig. 4 & 5 are only due to the aerodynamic coupling considered in the latter case.

Aeroelastic natural frequencies calculated using the FEM model of this wind turbine are reported in Ref. [10] which are shown in Fig. 6. All vibration modes except tower bending modes change with an increase in wind velocity. Lag modes in Fig. 5 & 6 follow the same trend with increasing wind velocities. Flap modes decrease with an increase in wind velocity in Fig. 6, whereas in Fig. 5, only the collective and regressive flap modes are decreasing with

Table 1. Comparison of natural frequencies

Mode	Natural frequency (Hz)	
	FEM	13 DOF Model
Tower fore-aft (α)	0.3240 *	0.3237
Tower side-to-side (β)	0.3120 *	0.3291
Yaw motion (γ)	-	6.8346
Drivetrain torsion (ψ)	0.6205 *	0.6099
Blade regressive lead-lag (θ_s)	1.0793 *	1.1170
Blade progressive lead-lag (θ_c)	1.0898 *	1.1399
Blade collective lead-lag (θ_0)	-	3.7978
Blade regressive flap (φ_s)	0.6664 *	0.6399
Blade progressive flap (φ_c)	0.6675 *	0.6542
Blade collective flap (φ_0)	0.6993 *	0.6879
Blade regressive torsion (ε_s)	-	5.5705
Blade progressive torsion (ε_c)	-	5.5738
Blade collective torsion (ε_0)	5.6 ~	5.5708

* From Ref.[8], ~ From Ref.[5]

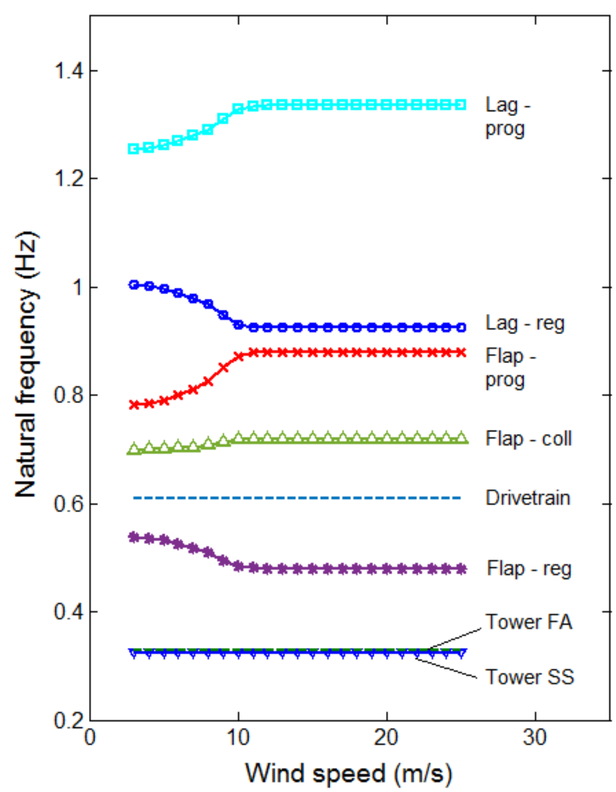

Figure 4. Natural frequencies variation considering rotational speed changes with wind velocities using 13 DOF model

increase in wind velocity. Aeroelastic flap modes will be accurately predicted by flexible beam models which captures aerodynamic coupling accurately. Differences in the aeroelastic natural frequencies reported in Fig. 5 and Fig. 6 arise due to simplification of flexible structure with rigid beam model and can be attributed to two reasons: centrifugal stiffening and aerodynamic loads. The rigid beam model doesn't account for centrifugal stiffening of the rotating beam in bending. In the current model, wind turbine blades are assumed as rigid beams with torsional spring attached at the blade root. If the blade is modeled as flexible, lower part of the blade vibrates with high amplitudes as it experiences higher loads and also it is less stiff when compared to the blade geometry near the root. So, rigid beam approximation for the blade doesn't take this into account.

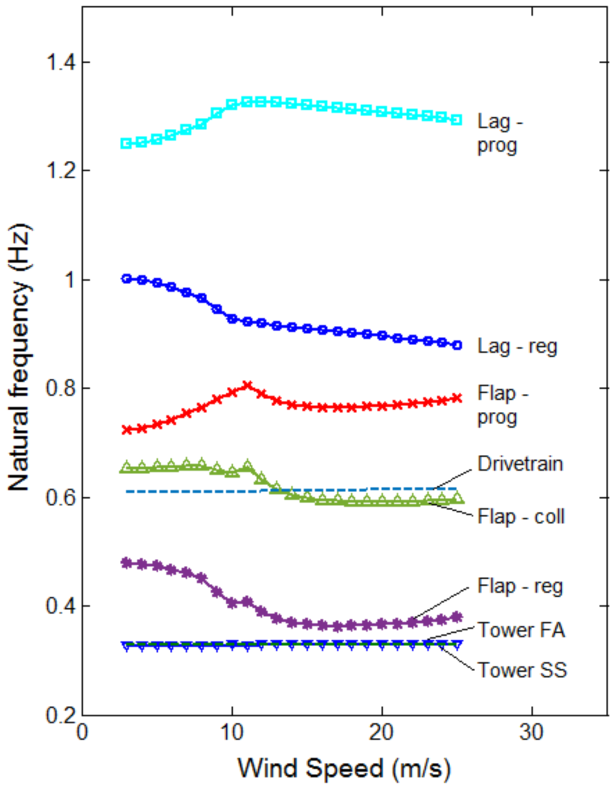

Figure 5. Natural frequencies variation considering aerodynamic coupling and rotational speed changes at various wind velocities using 13 DOF model

Wind turbine substructures experience periodic loads due to gravity, wind shear and tower shadow effects (ignoring turbulences and wind gusts). For a wind turbine with three blades, tower experiences loads with frequency equal to three times the rotational speed (denoted by 3P) due to the tower shadow effect. Structural loads (due to gravity and rotational effects) and aerodynamic loads exciting in-plane and out-of-plane vibrations of one blade over one full revolution for a wind velocity of 3 m/s are shown in Fig. 7. Structural loads in case of the blade in-plane vibrations are mainly produced by gravity effect and in case of out-of plane vibrations are mainly due to the rotational effects. Structural loads due to gravity dominate aerodynamic loads in case of blade in-plane vibrations, whereas aerodynamic loads are dominant in the case of out-of-plane blade vibrations. Tower shadow creates a sharp change in the aerodynamic loads whenever the blades come in front of the tower and in Fig. 7(b)&(d) the blade comes in front of the tower at an azimuthal position of 270˚.

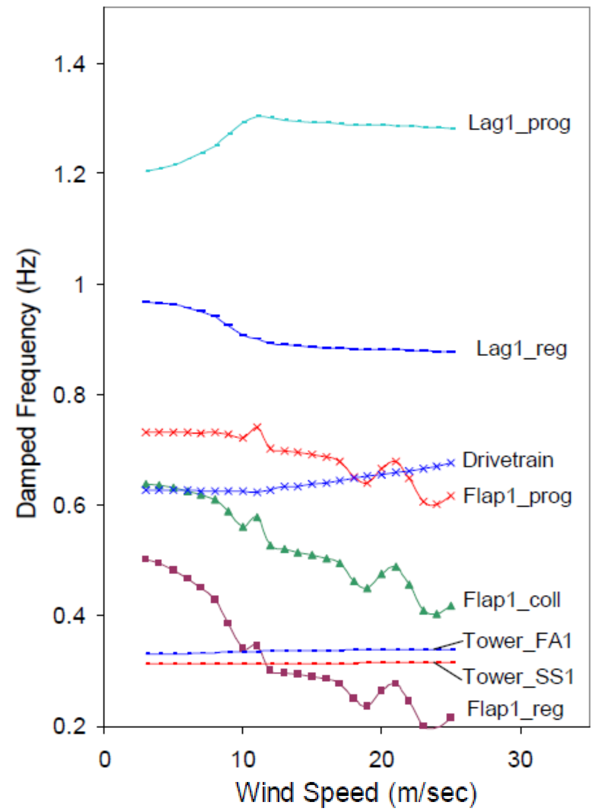

Figure 6. Natural frequencies variation considering aerodynamic coupling with FEM model of the NREL 5 MW model wind turbine [10]

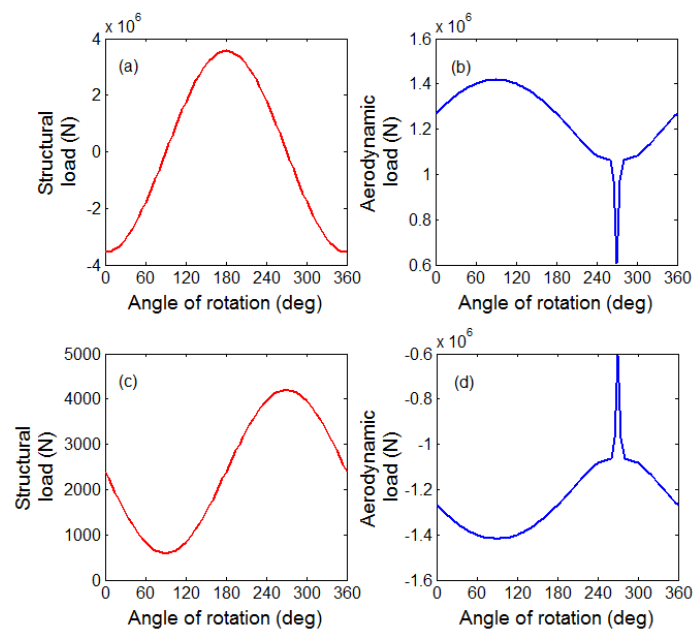

Figure 7. (a) & (b) Loads exciting blade in-plane vibrations, (c) & (d) loads exciting blade out-of-plane vibrations

As the tower and blades DOF are coupled in the EOM, loads exciting rotating blades will excite tower vibrations also. Tower fore-aft vibrations are excited by thrust forces acting on the blades and side-to-side vibrations are excitedby tangential forces acting on the blades. Structural loads generated due to gravity and rotation don't excite tower vibrations in case of symmetrical blades, as the summation of forces of the three blades becomes zero. Fast Fourier transforms (FFT) of the vibration responses at various wind velocities are shown in Fig. 8. Tower vibrations in Fig. 8(a)&(b) consist of 3P frequency and its harmonics which are excited by the tower shadow effect. Blade vibrations in Fig. 8(c)&(d) show dominant 1P frequency component and its harmonics. The synchronous component of the vibrations (1P) is excited by periodic loads (both structural and aerodynamic) shown in Fig. 7 and the harmonics of 1P are excited by sharp change in loads caused by the tower shadow effect. Blade's in-plane vibrations are mainly excited by periodic loads due to gravity whose magnitude is constant for all the wind velocities, thus the amplitude of the 1P frequency component in the in-plane blade vibrations at different wind velocities remains same. In the Fig. 8(d), the magnitude of the 1P frequency component of the blade out-of-plane vibrations increases with an increase in wind velocity due to two reasons: increasing structural loads due to increase in rotational speed and increasing aerodynamic loads due to wind shear at high wind velocities. Consideration of aerodynamic coupling in the model only changes damping and stiffness matrices as given in Eq. (22). So, structure vibrates with the same frequencies (harmonics of the rotational speed) when aerodynamic coupling is considered in the model. Some of the vibration frequencies (harmonics of the rotational speed) are close to the aeroelastic natural frequencies of the substructures and excite resonances. However, these resonances are highly damped and due to that their vibration amplitudes are less dominant than the amplitudes of 1P vibration frequencies.

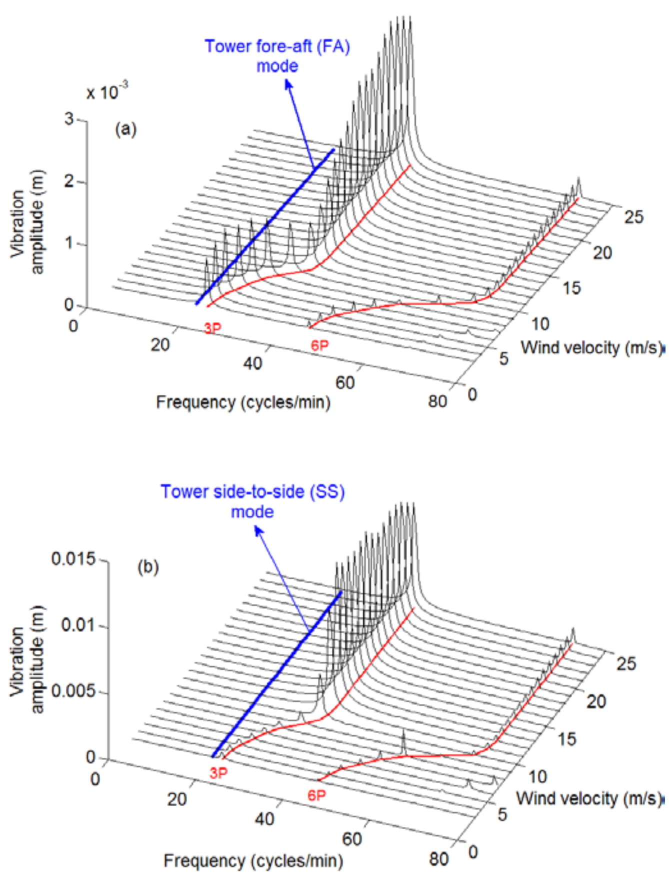

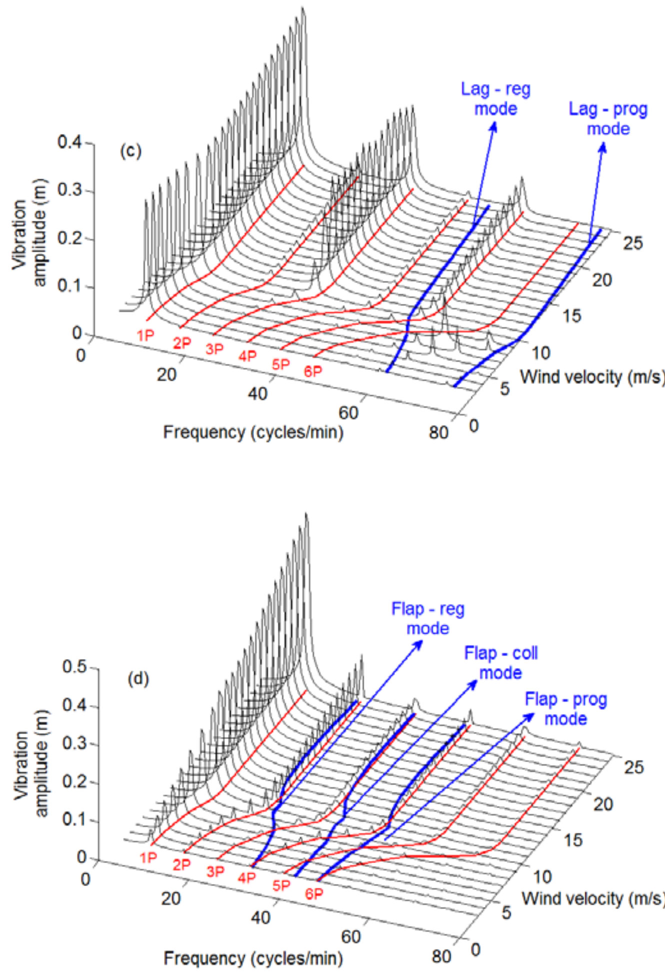

Figure 8. (a) Tower top fore-aft vibrations, (b) Tower top side-to-side vibrations, (c) Blade tip in-plane vibrations, (d) Blade tip out-of-plane vibrations

SUMMARY & CONCLUSIONS

The dynamics of the large wind turbine structure like NREL 5 MW model wind turbine are simulated by reducing it to a 13 DOF model. Natural frequencies and vibration responses at various wind velocities are predicted considering aerodynamic coupling with the structural behavior. Aeroelastic natural frequencies of the current and FEM models for increasing wind velocities follow the same trend (except progressive flap and drivetrain torsion) with an offset in the predicted values. This offset is due to the lack of the centrifugal stiffness effect created by the rotating beam in bending and inaccurate estimation of the aerodynamic coupling with rigid beam approximation. Using this model, the dynamics of the wind turbine can be simulated with less computational effort at the cost of accuracy. This model can be further improved by considering modal functions instead of the rigid beam approximation to represent flexible beam vibrations, wherein centrifugal stiffening and the appropriate aerodynamic coupling will be included in the model, which improves accuracy without increasing the number of DOF in the model.

REFERENCES

[1] Chopra, I., "Nonlinear dynamic response of wind turbine rotors", *PhD thesis, Massachusetts Institute of Technology*,

1977.
[2] Chopra, I. & Dugundji, J., Non-linear dynamic response of a wind turbine blade, *Journal of Sound and Vibration*, 63(2), 265-286, 1979.
[3] K. T. Kim, C. W. Lee, J. P. Park and J. H. Lee, Stability analysis of large-scale wind turbines considering non-symmetric configuration of rotor blades, *Proceedings of the 10th International Conference on Motion and Vibration Control*, 17-20 August 2010, Tokyo, Japan, 2010.
[4] Ramakrishnan, V and Feeny, B. F., In-plane nonlinear dynamics of wind turbine blades, *Proceedings of the ASME 2011 IDETC/CIE*, 28-31 August, Washington, USA, 2011.
[5] K. T. Kim and C. W. Lee, Coupled bending and torsional vibration analysis of flexible wind turbine blades by using assumed modes method, *15th International Congress on Sound and Vibration*, 6-10 July, Daejeon, Korea, 2008.
[6] Bir, G. S., User's guide to MBC3: Multi-blade coordinate transformation code for 3-bladed wind turbine, *National Renewable Energy laboratory*, Technical report, NREL/ TP-500-44327, 2010.
[7] Martin O. L. Hansen, Aerodynamic of wind turbines, Second Edition, 2008.
[8] Jonkman, J., Butterfield, V., Musial, W. and Scott, G., Definition of a 5-MW reference wind turbine for offshore system development, *National Renewable Energy laboratory*, Technical report, NREL/TP-500-38060, 2009.
[9] Bir, G. & Jonkman, J., Modal dynamics of large wind turbines with different support structures, *National Renewable Energy laboratory*, Technical report, NREL/ CP-500-43045, 2008.
[10] Bir, G. & Jonkman, J., Aeroelastic instabilities of large offshore and onshore wind turbines, *National Renewable Energy laboratory*, Technical report, NREL/CP-500-41804, 2007.

APPENDIX: Transformation matrices

$$T_X(\alpha)=\begin{bmatrix}1 & 0 & 0\\ 0 & cos(\alpha) & -sin(\alpha)\\ 0 & sin(\alpha) & cos(\alpha)\end{bmatrix}$$

$$T_Z(\beta)=\begin{bmatrix}cos(\beta) & -sin(\beta) & 0\\ sin(\beta) & cos(\beta) & 0\\ 0 & 0 & 1\end{bmatrix}$$

$$T_Y(\gamma)=\begin{bmatrix}cos(\gamma) & 0 & sin(\gamma)\\ 0 & 1 & 0\\ -sin(\gamma) & 0 & cos(\gamma)\end{bmatrix}$$

$$T_Z(\omega t+\psi)=\begin{bmatrix}cos(\omega t+\psi) & -sin(\omega t+\psi) & 0\\ sin(\omega t+\psi) & cos(\omega t+\psi) & 0\\ 0 & 0 & 1\end{bmatrix}$$

$$T_Z(\theta_i)=\begin{bmatrix}cos(\theta_i) & -sin(\theta_i) & 0\\ sin(\theta_i) & cos(\theta_i) & 0\\ 0 & 0 & 1\end{bmatrix}$$

$$T_Y(\varphi_i)=\begin{bmatrix}cos(\varphi_i) & 0 & sin(\varphi_i)\\ 0 & 1 & 0\\ -sin(\varphi_i) & 0 & cos(\varphi_i)\end{bmatrix}$$

$$T_X(\varepsilon_i)=\begin{bmatrix}1 & 0 & 0\\ 0 & cos(\varepsilon_i) & -sin(\varepsilon_i)\\ 0 & sin(\varepsilon_i) & cos(\varepsilon_i)\end{bmatrix}$$